HEAT TRANSFER ENHANCEMENT FROM BOUNCING BUBBLE DYNAMICS

David B. DONOGHUE*, Yann. M. C. DELAURÉ, Anthony J. ROBINSON*, Darina B. MURRAY*,**

* Dept. Mechanical & Manufacturing Engineering, Trinity College Dublin, Dublin 2, Ireland

** School of Mechanical and Manufacturing Engineering, Dublin City University, Glasnevin, Dublin, Ireland

Abstract. Heat transfer enhancement resulting from the effects of two phase flow can play an important role in for convective cooling. Currently, the effect of bubble/surface interactions has received very little attention. To address this, this paper investigates the effect of a single bubble bouncing on a heated surface. Local heat transfer measurements have been performed for two bubble release heights of 15 and 25 *mm*, along with two levels of surface heat flux, 5800 W/m^2 and 9040 W/m^2. High-speed photography and infrared thermography have been employed to investigate the path of the bubble and the resulting heat transfer effect when an interaction between the bubble and the heated surface takes place.

1. INTRODUCTION

Two phase flow plays an important role in heat transfer enhancement. Developments in two phase flow technology have allowed for ever more efficient heat exchangers, chemical reactors and simple cooling devices. Bubbly flows also have been used in non-heat transfer related problems such as froth flotation devices. In two phase bubbly flow, some heat transfer can be attributed to latent heat, but a study by Yoon et al. [1] estimated that bubble dynamics were responsible for up to 80 % of the total heat flux in nucleate boiling. Growing bubbles, whether they are gas or vapour, detach from a surface and in many cases subsequently come in contact with flat surfaces of a heat exchanger. This effect is known to increase heat transfer from the surface as shown by Donnelly et al. [2]. This enhancement effect is dependent on the surface characteristics, such as roughness, surface temperature and on the size and shape of the bubble.

Bubble growth and detachment has received a lot of attention in recent years, whether for horizontal or vertical surfaces. Quasi-static formation of bubbles is of importance and has been investigated by Oguz and Prosperetti [3] and more recently by Di Marco et al. [4, 5] and Duhar and Colin [6]. There are two important phenomena in bubble growth, static and dynamic growth. In static growth, inertia and viscous forces have a negligible effect, while in the dynamic regime inertia and viscous forces play a very dominant role. For gas bubbles, heat and mass transfer are neglected and gas dissolution is deemed negligible, whereas for vapour bubbles these phenomena must be accounted for.

Bubble induced heat transfer is not only confined to the nucleation of the bubble, but also the detachment, rise and subsequent impact of the bubble on a surface. A study by Cornwell [7] on horizontal tube arrays in R113, demonstrated that small bubbles nucleated from the lower tube surfaces. It was observed that when the upper tubes were at too low a temperature for the possibility of nucleation, large heat fluxes were observed; this was primarily due to a stream of bubbles passing over the tubes. These bubbles initiated from lower tubes and caused a local increase in the liquid velocity.

Bubbles sliding on a heated surface have been investigated by numerous authors. Qui and Dhir [8] used holographic interferometry to visualize both the near and far wake of the bubble for angles of plate inclination of 15° and 75° from the horizontal. At 15°, vortices were observed to form downstream of the bubble, detach, and move into the bulk fluid where they dissipated. This resulted in an increase in local heat transfer as heated fluid is moved away from the surface and cooler fluid replaces it. PIV measurements have also been used by Qui and Dhir [8] to observe the flow field around a sliding bubble moving under a heated inclined plate at 30°. The results obtained indicated that liquid at the front of the bubble is pushed outward, away from the heater surface, while at the rear of the bubble, liquid is pulled inwards creating a vortical structure in the wake. An investigation by Donnelly et al. [2], used thermochromic liquid crystals (TLC's) in conjunction with a high speed camera to obtain a time varying 2D temperature map of the heated surface. It was found that the bubble wake was responsible for the main heat transfer enhancement effect. The bubble wake was found to have the ability to increase the heat transfer coefficient by a factor of two.

The dynamics of bubbles impacting on surfaces has been the subject of some study. An investigation by Malysa et al. [9], found that bubble collision with liquid/gas and liquid/solid interfaces leads to rapid shape oscillation at high frequencies, followed by numerous bounces on the surface. With an increase in the fluid surfactants, the amplitude of the bubble shape pulsations and bouncing decreased. The effect of the hydrophobicity of the solid surface was also investigated. In the case of a hydrophobic surface, Teflon, the bubble attachment was not immediate, whereas for a hydrophilic glass surface numerous bounces were observed, also a delayed attachment to the surface was observed. Experiments were conducted in distilled water, n-pentanol, n-butanol and n-octanoic acid. A study by Suñol and González-Cinca [10] investigated gas bubbles impacting on ethanol-air surface. It was found that the bubble centroid movement was similar to that of a damped oscillator. Also found was a linear relationship between bouncing times and a corresponding Weber number. The following papers only deal with bubble dynamics, currently very little, to no information has been presented on the effect on heat transfer resulting from bouncing bubble dynamics.

The primary objective of this research is to contribute to the current understanding of heat transfer enhancement from a heated horizontal surface subject to a bouncing bubble. The surface is hydrophilic and the working fluid is ultra-pure water. The work presented here is for surface heat flux of 5800 W/m^2 and 9040 W/m^2, with an air bubble of approximately 3.8 ± 0.1 *mm* equivalent diameter. Whole field temperature measurement of the test surface is achieved using a Flir SC6000 high speed infrared (3-5 μm) thermography system. Bubble dynamics are analysed using two synchronised, mutually perpendicular high-speed cameras, which, through mathematical analysis, reveal the three-dimensional motion of the bubble.

2. EXPERIMENTAL SETUP

The experimental apparatus shown in Fig. 1 and 2 consists of a tank of 110 *x* 95 *x* 195 mm^3 constructed from 3 *mm* thick glass, with a horizontal test section. The tank contains a bubble injection point and a heated surface. Aluminium structural elements support the tank, allowing a high speed infrared camera to be mounted above the heated surface, while two CCD cameras are mounted horizontally at the sides of the test section as shown in Fig. 1.

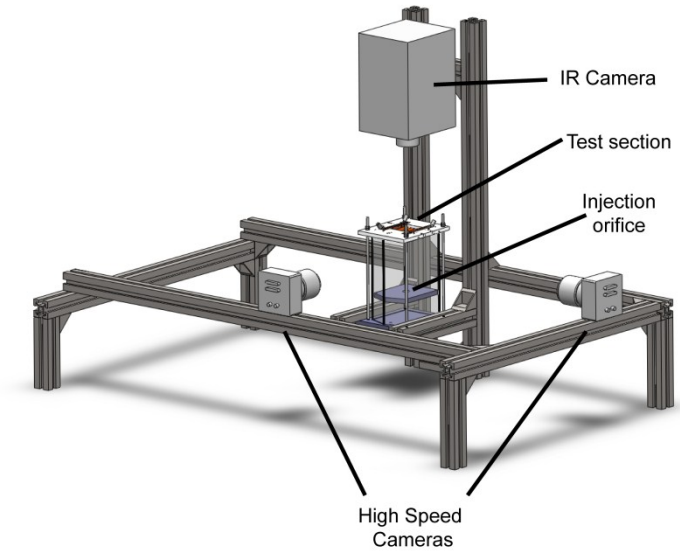

Fig. 1 Experimental apparatus

The injection point is on a movable platform, which allows the injection point to be adjusted to varying distances from the test surface. The test surface measures 60 *x* 84 mm^2 and consists of an electrically heated foil covered by a 10 μm paint layer and insulated by a 3 *mm* air gap that separates the foil from a 1 *mm* thick IR transparent glass (Fig. 2, a). The foil is 10 μm thick Constantan Alloy Cu55/Ni45 rolled foil supplied by Goodfellow Ltd. The foil is bonded between two bus bars using silver based electrically conductive glue (Loctite 3888 silver infused epoxy). The rear face of the foil is sprayed with a matt black paint with a high

emissivity. The polished IR transparent window is Calcium Fluoride (CaF_2) glass and has a percentage transmissibility of 95 % between 3-5 μm at a thickness of 1 *mm*.

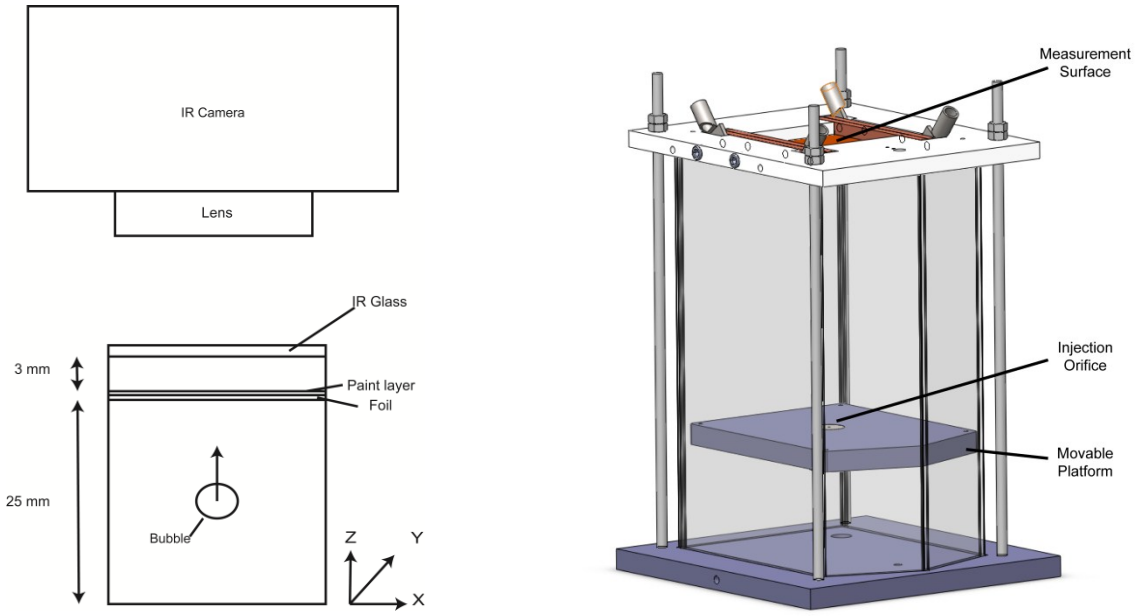

Fig. 2. a) Cross section of experimental surface. b) Completed rig.

To capture high speed phenomena, high intensity lighting is required to enhance the visibility of the bubble. This is provided by three high intensity light emitting diode (LED) strips (15 bulbs per strip) mounted behind each camera. A diffusive screen allows for a uniform light sheet to be acquired by the cameras. Two NAC Hi-Dcam II digital high-speed colour cameras were used in these experiments (max resolution 1280 x 1024 pixels, dependant on frame rate).

A FLIR SC6000 high resolution, high frame rate infrared camera was used in these experiments. It is used in conjunction with a high speed data recorder (HSDR) and camera controller computer. FLIR's SC6000 camera controller and ExaminIR frame grabber software were both used to acquire the data. The camera has a 640 *x* 512 pixel focal plane array (FPA) sensor which is vacuum sealed in a cooler assembly. The camera is set to record a zone that is 240 *x* 228 pixels in size, with an offset from the centre of the lens; this is chosen to reduce camera reflection from the IR window. The SC6000 is set to acquire frames at a frequency of 500 *Hz* with an exposure time of 1.2 *ms*. To achieve this, a Thurlby Thandar TG300 series function generator produces a square wave signal at 500 *Hz*. When the InSB IR sensor is active a square wave signal is sent from the camera to the PCI controller card for the first (master) Hi-Dcam camera, which in turn triggers the second (slave) camera. The Hi-Dcam cameras record at a frequency of 1000 *Hz* with an exposure time of 0.5 *ms*. This exposure time allows the bubble's detailed movements to be fully captured.

An accurate bubble injection rate is achieved by using a kdScientific model 200 infusion pump in conjunction with a Hamilton GASTIGHT 1002 2.5 *ml* syringe.

3. EXPERIMENTAL PROCEDURE

The tank is filled with ultrapure water which is maintained at 22 *°C*. An air injection rate of 100 *mlph*[1] was chosen for the experiment along with an injection orifice of 1 *mm*. The foil is electrically heated using a Lambda d.c. power supply, with a constant amperage of 20 and 25 *Amps* respectively for the two heat flux levels, and is allowed to settle for 3 minutes until a constant surface temperature has been achieved. This also allows the 3 *mm* air gap to reach a stable temperature. Once both the infrared and high speed cameras are armed and synchronized, a single bubble is injected into the test section and the instrumentation is triggered.

[1] This rate was chosen due to the limited recording time available for the high-speed cameras.

Once the images have been acquired the test section is allowed to cool back to 22 °*C*, before repeating the test.

4. ANALYSIS

The foil is ohmically heated, to achieve a uniform surface temperature. In order to calculate the heat convected from the foil to the fluid, an energy balance has been utilized. To complete the energy balance three assumptions are required, namely that a uniform heat flux is generated in the foil, that the temperature is uniform through the foil thickness and that the air between the foil and IR glass is stagnant so that one dimensional conduction across the air gap can be assumed.

To validate the assumption that the temperature on the bottom surface of the foil, in contact with the fluid, can be equated to that measured on the top surface of the foil, the Biot number criterion is assessed:

$$Bi = \frac{h\frac{\delta_{cn}}{2}}{k_{cn}} \ll 0.1 \tag{1}$$

where h is the heat transfer coefficient, δ_{cn} is the foil thickness and k_{cn} is the thermal conductivity of Constantan. For the current set up a Biot number of $Bi \approx$ 2.8e-4 has been observed [11], which is far below the threshold in equation 1. Along with the Biot number the foil time constant has been calculated and is $\tau \approx$ 1.8 e-5. The time constant characterises the response of the foil to an input, both these numbers allow an energy balance to be performed. This analysis does not take account of the effect of the paint layer. Further investigation needs to be performed in this area.

In the energy balance, uniform heat generation is assumed for each element, *dx* of the foil. When a spatial temperature gradient exists (due to the influence of the bouncing bubble in this case), there is heat conduction from warmer to cooler regions; also there is a change in the foil energy storage term, which is also temperature dependent. In order for the heat convected to the water to be determined an element by element analysis is performed using the following equation:

$$q_{generated} = q_{convected} + q_{lateral,cond} + q_{capacitance} + q_{cond,air} + q_{radiation} \tag{2}$$

from this equation the energy convected to the fluid can be found, and a resulting heat transfer coefficient found for natural convection as well as for when the bubble bounces on the surface.

$$q_{generated} = I_{el}^2 R_{el}\ ;$$

$$q_{capacitance} = m_{el} C_{p,cn} \frac{dT}{dt};$$

$$q_{radiation} = \epsilon\sigma(T_s^4 - T_\infty^4) \times dx^2$$

$$q_{lateral,cond} = -k_{cn}\delta_{cn}\nabla^2 T \times 4\delta_{cn} dx;$$

$$q_{cond,air} = -k_{air}\frac{dT}{dz} \times dx^2; \tag{3}$$

Where I_{el} is the current through one foil element of resistance R_{el}. k_{cn} and δ_{cn} are the Constantan thermal conductivity and thickness, while m_{el} and $C_{p,cn}$ are the mass and specific heat capacity of an element. One dimension, linear conduction has been assumed for the 3 *mm* air gap between the foil and the IR glass. ϵ is the emissivity, firstly the foil and secondly for the paint covering the foil. T_∞ is the temperature of the fluid and the IR glass over the foil. In this analysis the effect of the effect of the capacitance of the paint has been omitted and requires further investigation. The heat transfer coefficient between the foil and the fluid is as follows:

$$h = \frac{q''_{convected}}{\Delta T} \tag{4}$$

where,

$$q''_{convected} = \frac{q_{convected}}{dx^2} \tag{5}$$

where ΔT is the temperature difference between a foil element and the bulk water temperature.

In order to calculate the bubble position in space, successive images of the bubble are analysed using code written in Matlab©. To isolate the bubble from the background, images containing a bubble are subtracted from a reference image. From this resultant a threshold value is obtained, this threshold allows for accurate bubble boundary detection. Results are presented in time varying convective heat transfer coefficient; which has a calculated uncertainty of 15 %, based on a 95 % confidence limit.

5. RESULTS AND DISCUSSION

Results are presented with bubble position synchronised with heat transfer coefficient, for varying surface heat flux and bubble injection position. For all tests an injection orifice of 1 *mm* in conjunction with a constant injection flow rate of 100 *ml/hr* was employed. Two varying surface heat fluxes were investigated, along with two bubble release heights of 15 and 25 *mm* from the surface. The bubble volume is approximately 0.028 *ml*, which equates to an equivalent diameter of approximately 3.8 *mm*. To fully understand the effect of a bouncing bubble on heat transfer, the bubble dynamics will be shown followed by the resulting heat transfer. In total five experiments were done at each setting, so as to investigate experimental uncertainty.

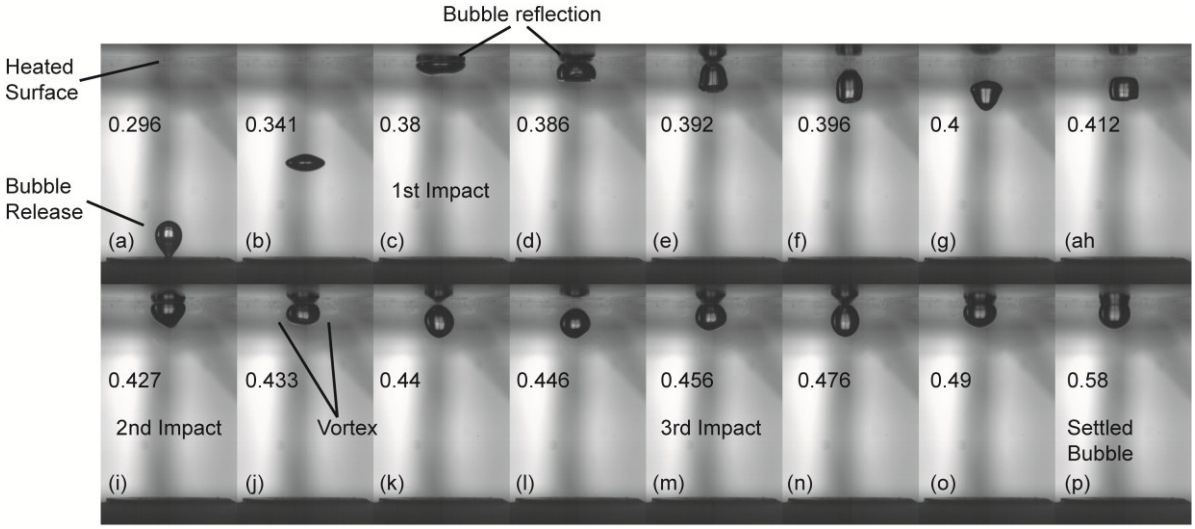

Fig. 3. Bubble growth/impact sequence a-p, the times are in second, with 0 seconds being the begining of the growth sequence for a release height of 25 *mm*

Fig. 3 depicts the bouncing of a 3.8 *mm* equivalent diameter bubble, from a release height of 25 *mm* and at the higher heat flux (H.H.F) of 9040 W/m^2. Large deformations can be seen as the bubble impacts and rebounds from the surface. It can be seen that the bubble bounces a total of three times on the surface, before attaching to the surface, while still continuing to oscillate. The bubbles reflection can be seen in the images; this is detected by code and removed from the images, so that bubble dynamics can be performed. Fig. 3, o shows the bubble resting a thin film of fluid before finally attaching to the surface at $t = 0.58$ *s*. The effect of this will be discussed later.

5.1. Bubble Dynamics

As the bubble enters the test section with a constant air flow rate of 100 *ml/hr*, the bubble is seen to oscillate. The injection process takes approximately 0.3 seconds as can be seen in Fig. 4. The bubble then takes almost 0.1 seconds to rise 25 *mm*. During the bubble rise there are significant shape oscillations. These oscillations in fact slow the bubble rise velocity, before accelerating it again. For a release height of 25 *mm*

four distinct peaks, between the $T_{TakeOff}$ and T_{Impact} lines are observed (Fig. 4, a), it was found that for a release height of 15 *mm* only two peaks was observed. Indicating that at a lower release height; the bubble has less time to oscillate.

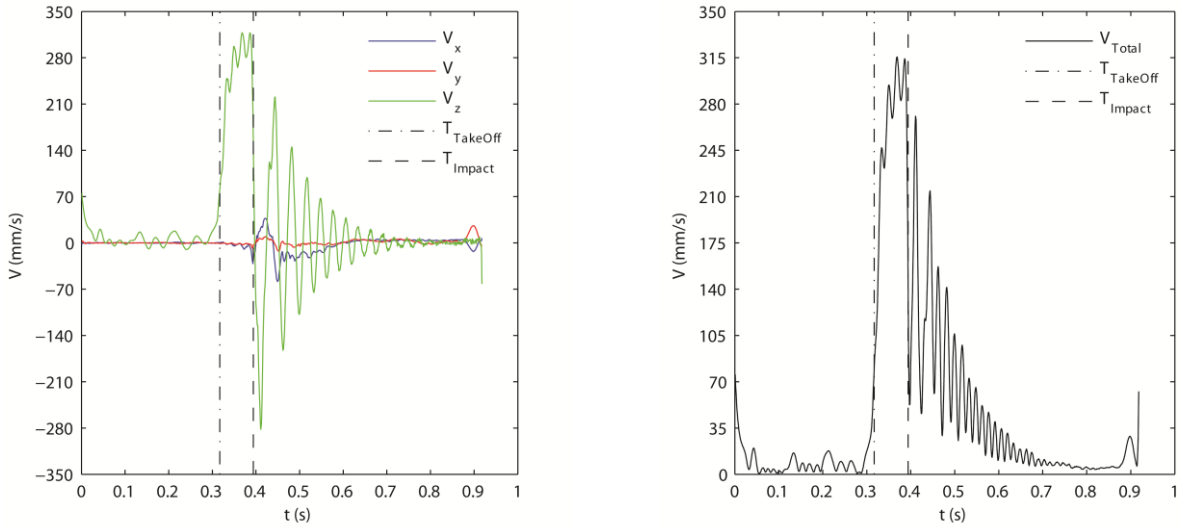

Fig. 4. a) Individual velocity componets. b) Resultant velocity. Height = 25 *mm*

Once the bubble begins to approach the surface; the upper surface of the bubble starts to cup. This cupping could possibly be due to fluid confinement between the bubble and the surface. The effect of this cupping will be discussed later. Once the bubble impacts the surface, large deformations take place. Firstly bubble initially flattens into a disk, before recovering its shape and rebounding from the surface. In this case (Fig. 4) the bubble bounced on the surface three times, before finally settling and attaching itself to the surface. The bubble bounced/slid a maximum of 1.5 and 1 *mm* in the *x* and *y* directions respectively, before finally settling. The extent and direction the bubble moved on the surface was found to be strongly dependent on the rise path. If the rise path were rectilinear, then only a slight translation was observed. However, if the bubble begins to tilt, one side of the bubble would impact prior to the rest of the bubble impacting; this caused the bubble to bounce unevenly. As the bubble rebounds from the surface, large surface oscillations were observed. These oscillations cause the bubble to invert itself, meaning that both the top and bottom surfaces are cupped in shape.

The thickness of the fluid film trapped between the bubble and the surface was investigated by Yan et al. [12] and was found to range from 100-200 μm. At t = 0.9 s (Fig. 4), there is a sudden increase in the bubble's x and y velocity components. This is where that trapped film disappears and the bubble attaches itself to the surface, resulting in the foil being in direct contact with the air in place of the liquid.

Fig. 5, a illustrates the individual acceleration components, a maximum acceleration of 4 x 10^4 mm^2/s is noted as the bubble impact the surface. After impacting the surface the bubbles tends to oscillate at a frequency of f = 25-40 Hz, until finally settling on the surface. Fig. 5, b shows the bubble centroid position and boundary outline from both cameras, up until the bubble impact the surface. The bubble shape can clearly be seen to deform and recover during its rectilinear path.

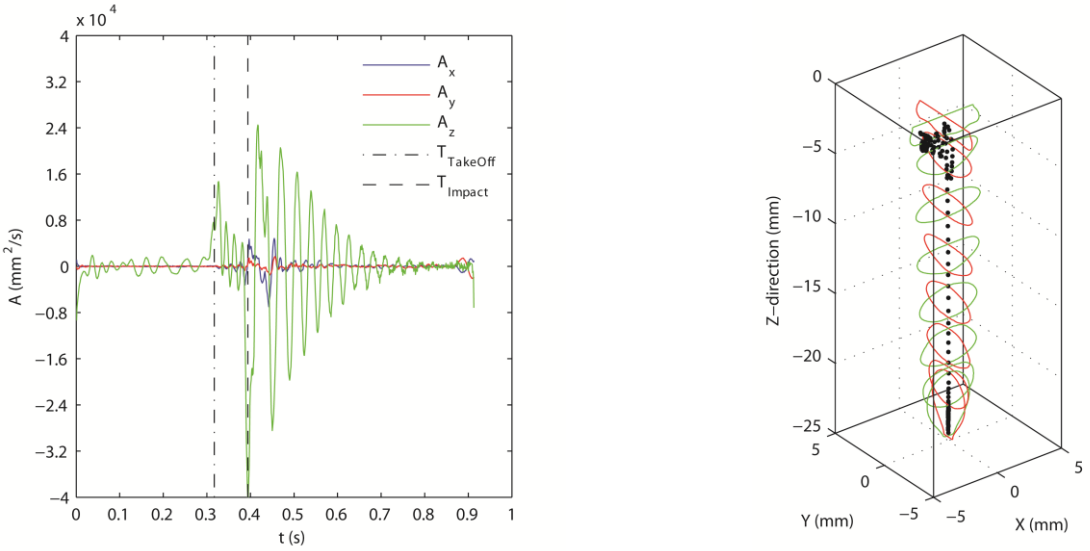

Fig. 5. a) Individual bubble acceleration components. b) Bubble boundary and centroid path (black dots), the green boundary corresponds to the master camera. Height = 25 *mm*

5.2. Temperature drop

For the two test settings, the heated foil dissipates 29 W and 45 W, which results in corresponding surface temperatures of approximately 35 °*C* and 45 °*C* and mean surface heat fluxes of around 5800 W/m^2 and 9040 W/m^2 respectively. Fig. 6 shows the variation in surface temperature across the foil just 6 *ms* after the bubble has impacted the foil, for a release distance of 25 *mm*, using a low heat flux. Fig 6, a displays lines of constant dimensionless surface temperature drop, as defined in equation (6), whereas Fig. 6,b shows surface temperature profiles at a specific instant in time. As previously discussed, as the bubble approaches the surface the bubble begins to cup. This cupping is evident in Fig. 6,b, as the extremities of the impact region exhibit a temperature drop of 1 °*C* , whereas the central point temperature drop is only half that. At 22 *ms* (Fig. 7) after impact, the temperature has dropped by 6 °*C*, although the centre of the bubble has a temperature drop of only 2 °*C*. This cupping and the effect of the bubble deformation was only evident when the release distance was 25 *mm*. At 15 *mm,* only a dome shaped temperature drop was observed.

The final shape prior to impact could be attributed to the maximum rise velocity achieved by the bubble. For a release distance of 25 *mm* a terminal rise velocity of 320 *mm/s* was found, whereas for a release distance of 15 *mm*, 280 *mm/s* was the maximum rise velocity. As the bubble approaches the foil, the fluid in front of the bubble must make way for the bubble. The greater the bubble velocity, the larger the effect of the fluid viscosity has on the bubble. This wall effect could be responsible for the cupping observed near the wall.

$$T_s = \frac{T_{s,bubble} - T_{Bulk}}{T_{s,t=0} - T_{Bulk}} \tag{6}$$

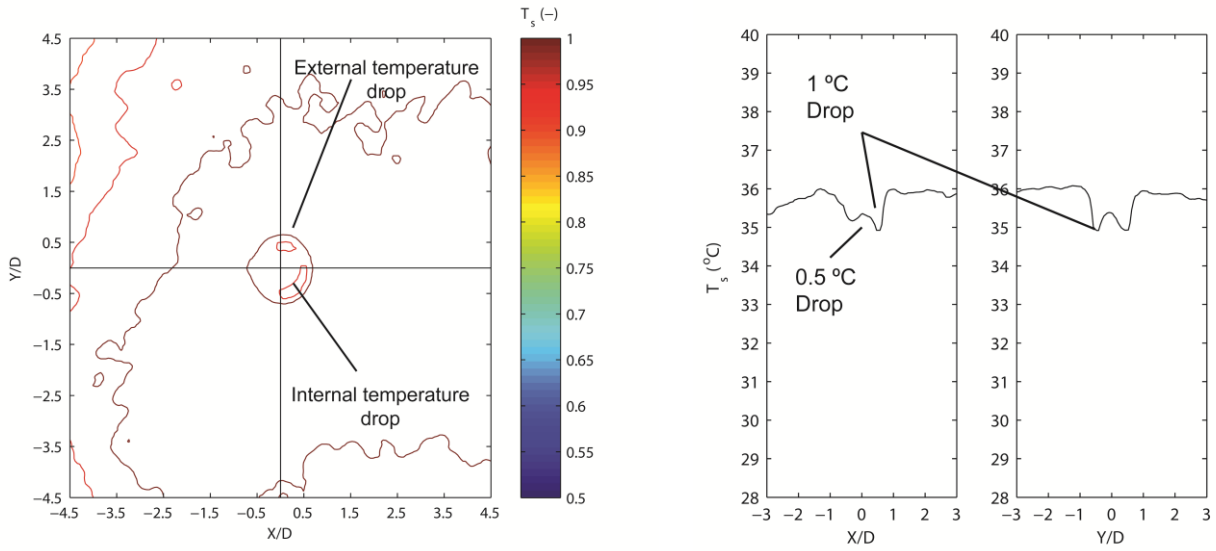

Fig. 6. Lower surface heat Flux (L.H.F). a) Dimensionless surface temperature contour plot 6 *ms* after bubble impact. b) Corresponding temperature profile in the *x* and *y* direction. Height = 25 *mm*

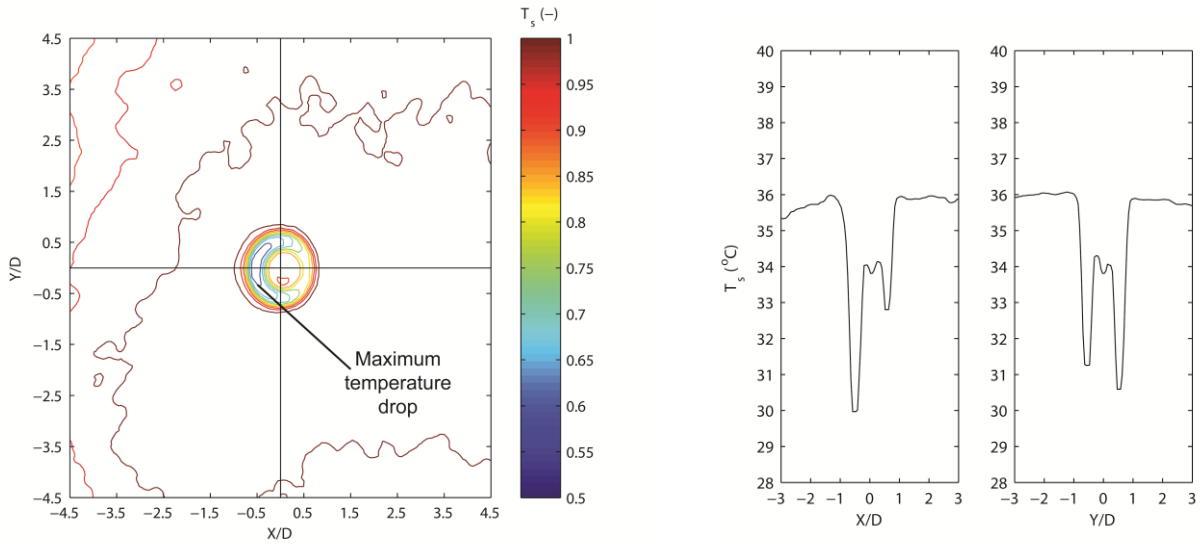

Fig. 7. Lower surface heat Flux (L.H.F). a) Dimensionless surface temperature contour plot 22 *ms* after bubble impact. b) Corresponding temperature profile. Height = 25 *mm*

As the bubble bounces on the surface, a minimum surface temperature of 27 °*C* was reached, which was confined to the edges of the bubble, whereas the central region had a corresponding temperature of 33 °*C* at that time. This minimum temperature drop occurred at a time of 72 *ms* after bubble impact in this case.

The continued bouncing action of the bubble reduces the temperature in the centre of the effected area, so that a dome shaped temperature profile is observed. In contrast to this example, for a release height of 15 *mm* a maximum temperature drop of 5 °*C* was found.

5.3. Heat Transfer Enhancement

For the two surface temperatures of 35 °*C* and 45 °*C*, natural convection heat transfer coefficients of 350 and 420 W/m^2K respectively have been calculated, for the steady state condition prior to the impact of the bubble. Once the bubble impacts the surface an immediate drop in surface temperature is observed, subject to the instrumentation time resolution of 2 *ms*. This drop in temperature results in a local increase in

heat transfer coefficient. Once the bubble has impacted the surface it deforms into a disk and immediately begins to recover its shape. As the bubble recovers, fluid mixing takes place. This can be observed visually, due to the density variation within the fluid (just visible in Fig. 3, j).

This density variation allows a vortex ring, which is created on impact, to be visually observed. This vortex ring follows the bubble during its first bounce; once the bubble returns to the surface this ring is pushed radially outward across the foil surface, with a portion of the warm fluid wafting downward, through the test section. This vortex ring extends to a maximum radius of one diameter. As the bubble continues to bounce the local heat transfer coefficient increases to a maximum of $h \approx 950\ W/m^2K$ for 25 *mm* release height and higher heat flux case; the enhancement effect at this time is shown in Fig. 8 a. This maximum enhancement occurs 72 *ms* after the initial impact of the bubble; at this time, the bubble is returning to the surface to complete its second bounce.

The heat transfer enhancement factor, ε, is defined as the ratio of the forced convection heat transfer coefficient measured during the bubble bouncing to that measured under natural convection conditions. This ratio allows for a more direct comparison of the heat transfer effect under varying test conditions.

$$\varepsilon = \frac{h_{Bubble}}{h_{Natural,Convection}} \tag{7}$$

Fig. 8 shows the effect of varying release height as well as varying heat flux. It was found that the enhancement effect of a bubble released at a height of 25 *mm* far outweighed that of a bubble released at 15 *mm*. An average, over numerous tests a heat transfer enhancement of approximately 2 is achieved by a bubble released 25 *mm* from the surface, whereas an enhancement of only 1.3 is achieved by a bubble released at 15 *mm*. This enhancement difference could be a result of the terminal velocity of the bubble, along with the depth of the boundary layer, in comparison to the release height.

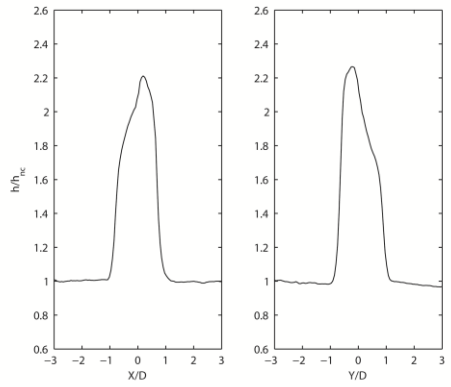

(a) 25 *mm* H.H.F. 72 *ms*

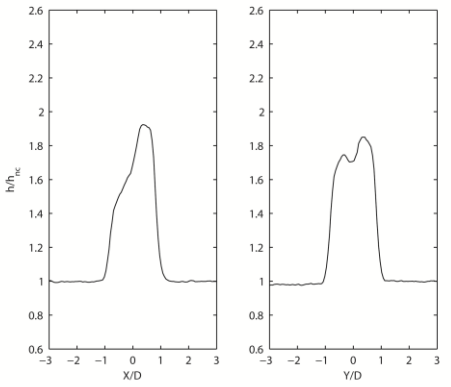

(b) 25 *mm* L.H.F. 76 *ms*

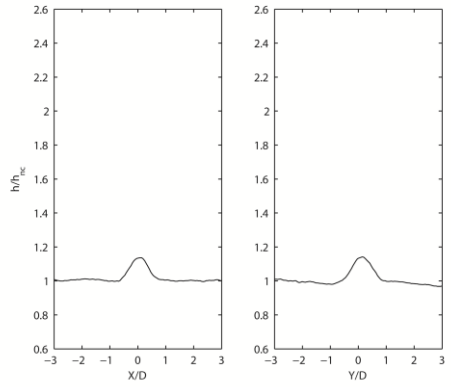

(c) 15 *mm* H.H.F 46 *ms*

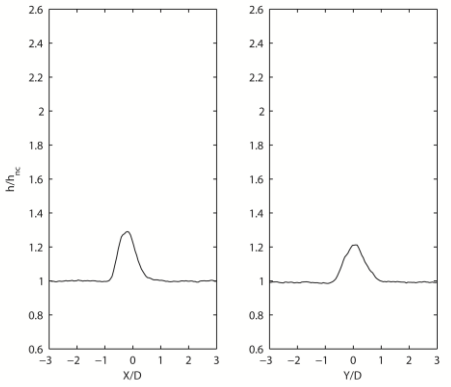

(d) 15 *mm* L.H.F. 256 *ms*

Fig. 8. Maximum heat transfer enhancement and times after bubble impact. a,b) 25 *mm* release height. c,d) 15 *mm* release height

In the four cases presented in Fig. 8 the final motion of the bubble in the *x* and *y*, direction was minimal, with a maximum travel distance of 2 *mm*. In addition, the free rise motion of the bubble was rectilinear in all cases. Fig. 9 illustrates the location and the projected maximum diameter of the bubble, when its enhancement effect was at its peak. The mean path of the bubble is to the upper left from the centre, while the area of maximum enhancement is to the lower right. This was found to be the case for all experiments.

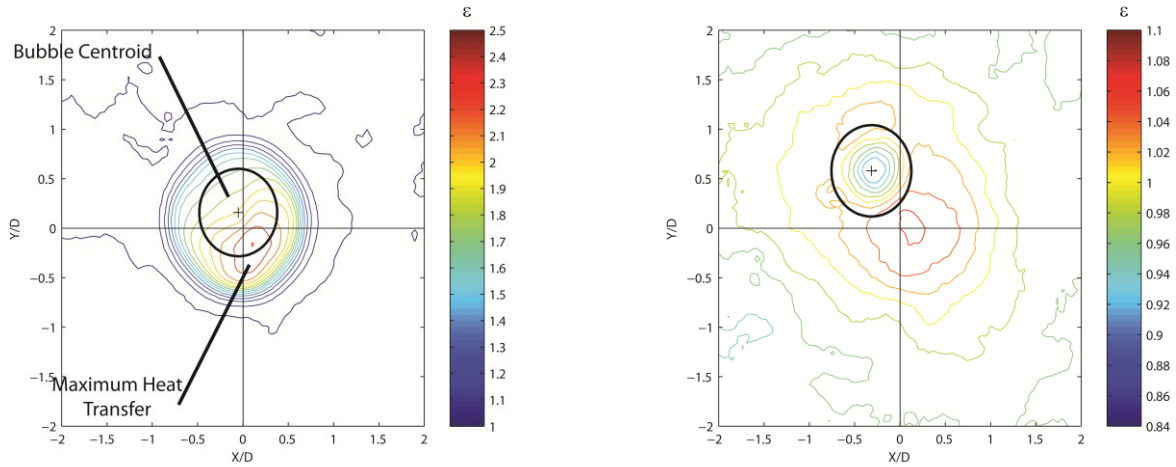

Fig. 9. a) Maximum heat transfer enhancement for a release height of 25 *mm* and high heat flux at $t = 72$ *ms* after bubble impact. b) Residual enhancement at $t = 4.6$ *s* after bubble impact. (change in scale)

It was observed that if the rise path of the bubble was not rectilinear, then the bubble path after impact would differ substantially to that of a rectilinear path. A maximum lateral travel of roughly 5 *mm* could be observed after impact in either plane. A desirable outcome of the increased travel was that the enhancement effect covered a larger surface area, therefore increasing the overall heat transfer.

At a time of 1.5-2 s after the initial impact, the bubble has settled on the surface and is stable, at this time the enhancement factor has diminished significantly. Once the bubble settles, the fluid film, which allowed the bubble to slide upon the surface, as seen in Fig. 4, has dried out. Therefore, the foil is no longer in contact with the water; instead, the air within the bubble is slowly heated. A consequence of this phenomenon is a reduction in the heat transfer coefficient within the contact patch of the bubble. Fig. 9, b shows this reduction in heat transfer associated with the bubble attaching to the surface. It is clear that there is a reduction in enhancement within the contact region of the bubble. The outline of the bubble shown in Fig. 9 is the projected extremities of the bubble rather than the contact patch on the foil surface.

6. CONCLUSIONS

From the results obtained in this study, is it clear that a bouncing bubble significantly increases the heat transfer from a horizontal heated surface, when compared to that of natural convection to the liquid. It was found that a maximum enhancement occurred at the larger bubble release height and higher heat flux tested. A possible explanation for this could be the difference in terminal velocity of the bubble between each case, as well as the ratio of the boundary layer depth to the release height and the associated volume of water. Thus, the terminal velocity was found to be higher for the greater release height and this corresponded with a larger volume of cool liquid. It was also found that the zone of maximum cooling was always slightly displaced from and in the opposite direction to the motion of the bubble. The formation of a vortex ring upon impact requires further investigation using stereo-PIV, so that the flow field around the bubble may be fully visualised.

7. ACKNOWLEDGEMENTS

The authors acknowledge the technical support staff of the Mechanical and Manufacturing Engineering Department of Trinity College Dublin.The project is funded by Science Foundation Ireland (SFI) grant number 09-RFP-ENM2151.

8. NOMENCLATURE

A	Acceleration (mm/s^2)
C_p	Specific heat capacity (kJ/kgK)
d_e	equivalent bubble diameter (mm)
f	frequency (Hz)
h	local convective heat transfer coefficient ($q''/(T_s - T_\infty)$) (W/(m^{2}K))
I	Foil current (A)
k	Conductivity (W/mK)
M_{el}	Mass(kg)
q''	Heat Flux (W/m^2)
q	Dissipated power (W)
Re	Reynolds number ($U_T D_e/\nu$)
R_{el}	Foil resistance (Ω)
T_s, T_∞	Surface and bulk fluid temperature (K)
t	time (s)
V	Velocity (V)
x, y	Plane coordinate (mm)
z	Vertical rise coordinate (mm)

Greek symbols

δ	Thickness (μm)
ε	Enhancement (-)
ϵ	Emissivity (-)

Subscripts

air	Air
cn	Constantan
cond	Conduction
el	Electrical

REFERENCES

1. Yoon, H., S. Koshizuka, and Y. Oka, Direct calculation of bubble growth, departure, and rise in nucleate pool boiling. International Journal of Multiphase Flow, 2001. **27**(2): p. 277-298.
2. Donnelly, B., T. O'Donovan, and D. Murray, Surface heat transfer due to sliding bubble motion. Applied Thermal Engineering, 2009. **29**(7): p. 1319-1326.
3. Oguz, H.N. and A. Prosperetti, Dynamics of bubble growth and detachment from a needle. Journal of Fluid Mechanics, 1993. **257**(-1): p. 111-145.
4. Di Marco, P., Birth, life and death of gas bubbles riding in a stagnant liquid, in Congresso Nazionale UIT sulla Trasmissione del Calore. 2005: Parma.
5. Di Marco, P., N. Forgione, and W. Grassi, Quasi-static formation and detachment of gas bubbles at a submerged orifice: Experiments, theoretical prediction and numerical calculations, in Congresso Nazionale UIT sulla Trasmissione del Calore. 2005: Parma.
6. Duhar, G. and C. Colin, Dynamics of bubble growth and detachment in a viscous shear flow. Physics of Fluids, 2006. **18**: p. 077101.
7. Cornwell, K., The influence of bubbly flow on boiling from a tube in a bundle. International Journal of Heat and Mass Transfer, 1990. **33**(12): p. 2579-2584.
8. Qiu, D. and V. Dhir, Experimental study of flow pattern and heat transfer associated with a bubble sliding on downward facing inclined surfaces. Experimental Thermal and Fluid Science, 2002. **26**(6-7): p. 605-616.
9. Malysa, K., M. Krasowska, and M. Krzan, Influence of surface active substances on bubble motion and collision with various interfaces. Advances in colloid and interface science, 2005. **114**: p. 205-225.
10. Suñol, F. and R. González-Cinca, Rise, bouncing and coalescence of bubbles impacting at a free surface. Colloids and Surfaces A: Physicochemical and Engineering Aspects, 2010. **365**(1-3): p. 36-42.
11. Incropera, F.P., D.P. DeWitt, T.L. Bergman, and A.S. Lavine, Fundamentals of heat and mass transfer, ed. I. John Wiley&Sons, New York. Vol. 6. 2007.
12. Yan, Y., D. Kenning, I. Grant, and K. Cornwell. Heat transfer to sliding bubbles under plane and curved surfaces. 1995: MEDICAL ENGINEERING PUBLICATIONS LTD.